Strong configuration interaction in the double ionization spectra of noble gases studied by the relativistic propagator method

Markus Pernpointner,* J. Patrick Zobel, and Nikolai V. Kryzhevoi
Theoretische Chemie, Universität Heidelberg, Im Neuenheimer Feld 229, D-69120 Heidelberg, Germany
(Received 14 October 2011; published 4 January 2012)

In this work, the four-component two-particle propagator technique is employed for the calculation of double ionization spectra of the noble gas atoms Ne through Rn. For a correct assignment of the individual final states, inclusion of spin-orbit coupling and electron correlation is mandatory and is accounted for in the framework of the relativistic propagator. It was observed that the $ns^2np^4(^3P_{2,1,0}, {}^1D_2, {}^1S_0)$ manifolds of all investigated noble gas dications exhibit a clear main-state character with only small admixture from other configurations. This also refers to the $2s^12p^5(^3P^o_{2,1,0}, {}^1P^o_1)$ states of Ne^{2+}. In the argon, krypton, and xenon dications, the $ns^1np^5(^3P^o_{2,1,0})$ states, and especially the $ns^1np^5(^1P^o_1)$ ones, lose intensity due to pronounced configuration interaction. These states experience strong mixings with ground-state shake-up satellites, which occupy the same energy region. The composition of the $5s^15p^5(^1P^o_1)$ singlet state of Xe^{2+} is studied in detail by analyzing the corresponding eigenvector. As long as a LS coupling picture can be approximately maintained, the amount of singlet-triplet splitting decreases in the sequence from neon to xenon. In the $6s^16p^5$ manifold of Rn^{2+}, a complete disappearance of well-defined main states takes place leading to a dense and complicated spectrum governed by very strong multiconfiguration effects. Relativistic corrections to the Coulomb interaction are accounted for by inclusion of the Gaunt (magnetic) term.

DOI: 10.1103/PhysRevA.85.012505 PACS number(s): 31.30.jc, 32.80.Fb, 31.15.vj

I. INTRODUCTION

Doubly charged ions play an important role especially due to their high reactivity and thus attract considerable interest [see recent special issue no. 41 on multiply charged ions in Phys. Chem. Chem. Phys. **13** (2011)]. Many experimental techniques are available for exploring properties of these species. Auger, optical, double-charge transfer, and charge-stripping spectroscopies as well as various coincidence methods are among them (see, for example, review papers [1,2]).

Noble gas atomic dications were in focus of numerous experimental and theoretical studies [3–23]. Except for some anomalies in the intensity distributions [8,9,13,15], the main states in the low-energy spectral regions of these ions describing the removal of the two outermost p electrons are well understood, which makes this class of dications excellent candidates for testing and calibration of new methods. The situation is more complex in deeper energy regions, where at least one of the emitted electrons belongs to the outermost s shell. Together with the main states, these regions contain numerous satellites, which interact with each other resulting in considerable intensity redistributions. Strong configuration interaction effects often prevent an unambiguous assignment of the electronic states there.

For quite a few states in the double ionization spectra of argon, krypton, and xenon, the assignment was not easy and deserved long debates. In particular, we would like to draw attention to the states at 14.76, 20.27, and 26.14 eV above the ground state of Xe III. Owing to restrictions to the wavelength ranges explored in early optical measurements, only the first state in the above sequence was assigned [24], namely, to the main state $5s^15p^5(^1P^o_1)$. By measuring the Auger spectra of xenon, Werme *et al.* [23] attributed the last two states to $5s^05p^6(^1S_0)$ and $5s^25p^35d(^1P^o_1)$, respectively. This interpretation was doubted by Hertz in his electron impact study [20] and later by Southworth *et al.* [18], who measured Auger spectra of Xe. The assignment made in the former work was based on the results of single configuration Hartree-Fock calculations. By carrying out multiconfiguration relativistic calculations, Aksela *et al.* [17] corroborated that the states at 20.27 and 26.14 eV should be reassigned as the satellite $5s^25p^35d(^1P^o_1)$ and the main $5s^05p^6(^1S_0)$ states, respectively. A new reassignment, this time concerning the first and the second states, was proposed by Persson *et al.* [16] after carrying out optical measurements and theoretical estimations. The lowest energy state was interpreted as the satellite $5s^25p^35d(^1P_1)$, followed by the main state $5s^15p^5(^1P^o_1)$. Note that this reassignment was adopted by Salomon [25] in his compilation of the energy levels of the neutral and ionic xenon and is currently used in the NIST database [26]. More recent experimental studies (see, e.g., Refs. [7,8]) followed, however, the interpretation by Southworth *et al.* [18] and Aksela *et al.* [17].

In the present study, the double ionization spectra of the noble gas atoms are calculated by means of a propagator method and the problem with the assignment of states in their inner-valence parts is reexamined. We exploit the algebraic diagrammatic construction (ADC) scheme for the two-particle propagator [27,28]. So far this method was extensively used exclusively for a nonrelativistic description of doubly ionized states (see, e.g., Refs. [29–32] and references therein). After the recent implementation by Pernpointner [33], an account for relativistic effects in double ionization spectra has become possible with ADC. In most of the earlier theoretical studies on the noble gas dications, the numerical multiconfiguration Dirac-Fock approach (MCDF) [34] was used, where, due to limited computational resources, only a restricted correlation space could be constructed. In numerical

*markus.pernpointner@pci.uni-heidelberg.de

approaches, the way for obtaining virtual orbitals necessary for building up the configuration interaction (CI) matrix is somewhat different to the methods employing atom-centered Gaussian- or Slater-type basis functions of increasing angular momentum. In the meantime, however, it has become possible to perform large-scale atomic MCDF/CI calculations (see, e.g., Refs. [35–41] and references therein). The ADC scheme avoids the drawbacks connected to truncated CI methods and utilizes large configuration spaces constructed from occupied and virtual Dirac-Hartree-Fock spinors, allowing for a good description of both static and dynamic correlation effects in addition to a detailed final state composition analysis. According to our calculations, the contribution of the $5s^15p^5$ configuration into the state at 14.76 eV is by far the largest one among all the $^1P_1^o$ states. Therefore, this state should be assigned as the main $5s^15p^5(^1P_1^o)$ state. When going from Xe to lighter atoms, the ambiguity in interpreting the main $ns^1np^5(^1P_1^o)$ state ($n = 2,3,4$ for neon, argon, and krypton, respectively) diminishes in agreement with previous studies.

It has to be pointed out that the correct assignment of the singlet $ns^1np^5(^1P_1^o)$ state has the direct influence on the magnitude of the energy gap between this state and the corresponding triplet $ns^1np^5(^3P^o)$. The knowledge of the singlet-triplet splitting is needed in various applications. By adopting the state interpretation mentioned in the previous paragraph, we obtain a smoothly decreasing singlet-triplet splitting $^1P_1^o - {}^3P^o$ with increasing atomic mass.

Rn^{2+} is the heaviest dication considered here. To the best of our knowledge, it has never been studied experimentally. The theoretical results for this system are also scarce and only exist for the outer-valence spectral region $6s^26p^4$ [42]. In the present study, we explore the inner-valence spectral region of Rn III for the first time. We see that neither the $6s^16p^5(^1P_1^o)$ state nor the $6s^16p^5(^3P^o_{2,1,0})$ ones can definitely be assigned. The composition of almost each dicationic state in the inner-valence region represents a strong mixture of several configurations with no prevailing one.

II. METHODOLOGY IN THE RELATIVISTIC CASE

The two-particle propagator or Green's function describing a double ionization or attachment process reads as

$$G_{pq,p'q'}(t_1,t_2;t_1',t_2') = -\left\langle \Psi_0^N \middle| \hat{T}[c_p(t_1)c_q(t_2)c_{q'}^\dagger(t_2')c_{p'}^\dagger(t_1')] \middle| \Psi_0^N \right\rangle, \quad (1)$$

with $|\Psi_0^N\rangle$ being the *exact* N-particle ground state wave function. In the case of the Dirac-Coulomb (DC) operator

$$\hat{H}_{DC} = \sum_{i=1}^{N}[c\vec{\alpha}_i \cdot \vec{p}_i + \beta_i m_e c^2 + V_{\text{ext}}(i)\mathbf{1}_4] + \sum_{i<j}^{N} \frac{1}{r_{ij}}, \quad (2)$$

there are no normalizable many-electron eigenfunctions [43–46] requiring the extra condition that the negative energy eigenstates are not accessible. In the formalism of relativistic propagators, we therefore work with a DC Hamiltonian that is projected onto the space of the positive-energy states allowing for a construction of a normalizable many-electron basis required in Eq. (1). $\hat{T}$ is the Wick time-ordering operator and the $c_q^\dagger(t)$ $[c_q(t)]$ denote creation (destruction) operators for one-particle states $|\phi(q)\rangle$ in the Heisenberg representation. As a consequence, the second quantization operators only act in the positive-energy space (no pair formalism; see, e.g., Ref. [47]) and refer to occupied and virtual one-particle states from which the many-particle wave functions are built.

For the practical implementation one starts from the energy-dependent representation of Eq. (1) obtained by a Fourier transformation:

$$\Pi_{pq,p'q'}(\omega) = \Pi^+_{pq,p'q'}(\omega) + \Pi^-_{pq,p'q'}(\omega).$$

$\Pi^+_{pq,p'q'}(\omega)$ hereby describes a two-particle attachment, whereas $\Pi^-_{pq,p'q'}(\omega)$ is used for a two-particle detachment (ionization) process. The Lehmann representation [48] of $\Pi^-_{pq,p'q'}(\omega)$, which we are starting from, reads as

$$\Pi^-_{pq,p'q'}(\omega) = -\sum_m \frac{x^{(m)}_{pq} x^{(m)*}_{p'q'}}{\omega + E_m^{N-2} - E_N^0 - i\eta}, \quad (3)$$

utilizing a set of fully correlated $N-2$ particle states $|\Psi_m^{N-2}\rangle$ in the positive-energy space with corresponding energies E_m^{N-2}. η is an infinitesimal positive number required for the convergence of the backtransformation. The spectral amplitudes

$$x^{(m)}_{pq} = \left\langle \Psi_m^{N-2} \middle| c_p c_q \middle| \Psi_0^N \right\rangle$$

provide information about the composition of the mth final state, with respect to the one-particle states p and q. It should be pointed out that the N-particle ground-state wave function $|\Psi_0^N\rangle$ can be expanded in a N-particle basis of Slater determinants made of four-component one-particle functions. The no-pair confinement puts us into the advantageous situation that the spin-orbital-based expressions derived from diagrammatic perturbation theory need not be modified for a corresponding realization with four-component one-particle functions.

Up to this stage we have not yet obtained actual expressions for the propagator. This is established by a combination of the diagrammatic representation for Π^- together with an algebraically formulated perturbation expansion of a nondiagonal representation of Eq. (3) termed as algebraic diagrammatic construction [27,28,30]. In a compact matrix notation, Eq. (3) reads as

$$\underline{\Pi}^-(\omega) = \underline{X}^\dagger(\omega\underline{1} + \underline{\Omega})^{-1}\underline{X},$$

with $\underline{1}$ being the identity matrix and $\underline{\Omega}$ being the diagonal matrix of double ionization potentials. This diagonal representation is now brought into a nondiagonal form by inserting a so-called intermediate state basis [49] leading to

$$\underline{\Pi}^-(\omega) = \underline{F}^\dagger(\omega\underline{1} - \underline{\Gamma})^{-1}\underline{F}.$$

A perturbational expansion of the $\underline{\Gamma}$ and $\underline{F}$ matrices then allows for an order-by-order comparison to the graphs obtained by a diagrammatic perturbation expansion from which the explicit expressions for the matrix elements can be derived [27,50]. The $\underline{F}$ matrices are needed for the calculation of transition moments and are disregarded for the current investigation. A final matrix diagonalization then yields the sought double ionization potentials together with the eigenvectors containing the expansion coefficients of the mth eigenstate in terms of the

intermediate basis. A specific eigenstate in the intermediate state basis can also be expanded in a perturbation series starting with a two-hole Slater determinant in zeroth order and where the additional terms account for electron relaxation and correlation [51]. If a specific final state exhibits main-state character, $3h1p$ configurations mix in only weakly, whereas other $2h$ configurations may participate substantially. For final states possessing higher energy, however, a clear one-particle-based interpretation of the double ionization process cannot be maintained any longer due to the accessibility of many additional excited $3h1p$ configurations being located in the same energy regime as an inner-valence doubly ionized final state. Therefore, the designated state will mix with many other states and the corresponding pole strength will therefore be distributed over many participating configurations. This is the same breakdown phenomenon as observed in the inner-valence single ionization processes [51,52]. After the diagonalization of the ADC matrix, the eigenvectors contain the configurational information of a specific final state in the $2h/3h1p$ space and reveal all mixing configurations in this space for the analysis of a possible breakdown situation. It should be noted that a $2h/3h1p$ configuration space may not be sufficient for the description of some high-lying or very weak satellites and an enlargement of the configuration space beyond $3h1p$ becomes necessary if one seeks a good description of these satellites.

In our analysis, emphasis lies on the ns^1np^5 final-state manifold of the doubly ionized noble-gas atoms and valuable information about the singlet-triplet splitting could be obtained. As in the one-particle case, the two-particle ADC matrix attains block structure, each block belonging to a different (bosonic) final-state symmetry. For atoms, the current implementation even supports *linear* symmetry ($D_{\infty h}$ and $C_{\infty v}$), which greatly alleviates final-state analysis. The various bosonic M_J projections are hereby described by separate ADC matrices and a $(2J+1)$-fold occurrence of identical eigenvalues in different M_J projections unambiguously allows the attribution of the corresponding eigenstate to a specific J value. In the corresponding eigenvector, the sum of the spinor m_j values contributing to a specific $2h$ or $3h1p$ configuration also gives M_J. A detailed description of the symmetry handling in Dirac-Coulomb ADC (DC-ADC) can be found in Ref. [33].

III. COMPUTATIONAL DETAILS

In order to obtain consistent results, it is necessary to investigate the effects of basis set size and active space dimensionality. The extended second-order DC-ADC(2e) treatment of double ionization energies normally bears a methodological error, which can reach 1 eV with respect to absolute peak energies. However, the energetic separations of the individual peaks are much better reproduced with a considerably smaller relative error. In general, nearly saturated bases and large active spaces have to be employed for a minimization of both the absolute and relative error. For high-energy, inner-valence ionizations, relaxation effects play a significant role and can prevail over correlation effects making a second-order method such as ADC(2e) less accurate. In order to arrive at maximum consistency and to eliminate additional errors introduced by too small basis sets and/or active spaces, we performed systematic tests for all noble gas atoms under consideration. For the errors in the *onset* of the double ionization with respect to experimental values from the NIST database, we obtain (in percent, electronvolt in parentheses) for Ne: 2.3% (1.42), Ar: 1.9% (0.80), Kr: 2.1% (0.79), Xe: 2.2% (0.71), and Rn: 1.9% (0.55). This points to a stable systematic error founded in the methodological approach. For the calibration of the basis sets and the active spaces, a common origin of the theoretical and experimental spectra was therefore chosen as demonstrated for Xe in more detail below. In all spectra, the *relative* error, which means the average deviation of the calculated final states from experimental data referred to a common origin, is much smaller and the basis sets and active spaces were optimized in order to minimize these relative deviations. For the xenon atom, the relative error amounts to 0.50% with similar values for the other noble gases. The accuracy of the dicationic excited states can therefore be considered sufficient in order to allow for a reliable interpretation of the calculated spectra.

We employed the triple and quadruple zeta basis sets by K. Dyall [53–55] in combinations with two active spaces comprising spinors from -10.0 to $+16.0$ a.u. (AS1) and from -10.0 to $+65.0$ a.u. (AS2), respectively. Additionally, two sets, S_1 and S_2, of polarization functions $2f1g$ and $3f2g1h$, respectively, were tested. Diffuse functions were checked not to influence the results noticeably because electron densities in dications are rather contracted and, therefore, were not used in the calculations. The results in Table I show the considerable stability of relative energies upon extension of the basis and active spaces. This behavior is of higher relevance than the absolute accuracy, thus rendering the DC-ADC technique a very useful tool for spectrum analysis. The final calculations for xenon were done with the tz-S_1-AS1 combination as a compromise between accuracy and computational cost. The corresponding results are discussed in the next section.

The same tests were undertaken for the other noble gas atoms and their outcomes are comparable to the above one. For Kr and Rn, the triple zeta Dyall bases [53–55] were chosen, whereas for neon and argon, individually optimized $11s6p2d1f$ and $16s12p3d2f1g$ sets were employed for the production runs.

In the NIST reference data table for Xe III [26], the $^1P^o$ value (marked by the asterisk) is attributed to an energetically high-lying final state, which would lead to quite an exaggerated value for singlet-triplet splitting in this manifold (LS picture assumed valid). The Xe III data published by Carroll *et al.* [7] were obtained from Xe $N_{4,5}OO$ Auger spectrum. In the next section, we discuss the DC-ADC results for xenon in detail and extend the analysis to the lighter homologues krypton, argon, and neon. At the end, we demonstrate the pronounced single configuration breakdown of the excited $Rn^{2+}6s^16p^5$ manifold in its DC-ADC spectrum.

IV. RESULTS AND DISCUSSION

A. Xe

According to Carroll *et al.* [7], the double ionization onset of the xenon atom is given as 33.105 eV, which is in reasonable agreement to our best obtained value of 32.393 eV considering the second-order character of the perturbational approach.

TABLE I. Energies (in eV) of the main states of Xe III relative to the $5s^25p^4(^3P_2)$ ground state for different basis sets, polarization functions, and active spaces (see text for details). For the energy level marked by the asterisk, there are different assignments in the literature. tz and qz denote triple and quadruple valence zeta.

			Active space AS1				Active space AS2				Reference	
Config.	Term	J	S_1 (tz)	S_2 (tz)	S_1 (qz)	S_2 (qz)	S_1 (tz)	S_2 (tz)	S_1 (qz)	S_2 (qz)	Ref. [7]	NIST [26]
$5s^25p^4$	^3P	2	0.0000	0.0000	0.0000	0.0000	0.0000	0.0000	0.0000	0.0000	0.0000	0.0000
		0	1.0488	1.0479	1.0483	1.0474	1.0494	1.0485	1.0492	1.0483	1.0081	1.0080
		1	1.1758	1.1830	1.1750	1.1821	1.1768	1.1840	1.1764	1.1834	1.2144	1.2143
$5s^25p^4$	^1D	2	2.1671	2.1502	2.1666	2.1496	2.1680	2.1510	2.1680	2.1509	2.1200	2.1200
$5s^25p^4$	^1S	0	4.6849	4.6691	4.6834	4.6676	4.6849	4.6711	4.6865	4.6707	4.4762	4.4762
$5s^15p^5$	$^3P^o$	2	11.8567	11.8287	11.8315	11.8013	11.8567	11.8285	11.8315	11.8011	12.1831	12.1830
		1	12.5780	12.5421	12.5460	12.5065	12.5778	12.5416	12.5456	12.5057	12.8409	12.8408
		0	13.2175	13.1878	13.1827	13.1474	13.2186	13.1890	13.1860	13.1514		13.4317
$5s^15p^5$	$^1P^o$	1	15.0138	14.8935	14.9244	14.8015	15.0096	14.8891	14.9180	14.7949	14.7574	20.2748*
$5s^05p^6$	^1S	0	26.9003	26.7845	26.8572	26.7381	26.8998	26.7839	26.8571	26.7379	26.1430	26.1430

The computed DC-ADC(2e) stick spectrum for Xe shown in Fig. 1 exhibits well-separated regions. The first group of lines between 32.39(0.0) and 37.07(4.69) eV (the numbers in the parentheses correspond to the relative energies with respect to the ground state of Xe^{2+}) consists of main states derived from the $5s^25p^4$ ground-state configuration of the Xe^{2+} ion. Hereby, the ^3P term is spin-orbit split into a $J = 2,1,0$ multiplet. It is important to note that in the absence of an external magnetic field, a $2J + 1$ degeneracy pertains, which is numerically reproduced in a DC-ADC calculation employing linear symmetry (see above). The eigenvalues for the $^1D_2$ and $^1S_0$ final states, therefore, occur five times and once, respectively, in the calculations. All five states in the first group acquire a pole strength larger than 0.85 and clearly represent main states. The experimental order of the J multiplets is reproduced and the energy separations are in good agreement to the spectroscopical observations (see Table I).

The next group of lines represents final states originating from a $5s^15p^5$ configuration leading to the $^3P^o_{2,1,0}$ states and to a proposed $^1P^o_1$ term at 47.41(15.01) eV. The latter will be discussed below in more detail due to some ambiguity in its interpretation that is mainly caused by a considerable loss of a main state character. To this group of lines we assign also numerous satellites spreading over the energy region up to about 56 eV. Most of these states are of the $5s^25p^3nl$ character. Strong interaction of some satellites with the $^3P^o_{2,1,0}$ and $^1P^o_1$ main states giving rise to a pronounced spectral intensity redistribution will also be addressed below. We would like to note that in the ADC(2e) method, satellites are treated consistently through the first order only. As a result, their energies exhibit a larger deviation from the corresponding experimental values than the main states, which are treated through the second order of perturbation theory. In the present study, these overestimations in energy mainly apply to the satellites, including the lowest-energy multiplet $5s^25p^35d(^5D^o_{3,2,4,1,0})$, which acquires only negligible intensity in the computed spectrum and the strongest satellites of $5s^25p^35d(^3P^o_{0,1,2})$ and $(^1P^o_1)$ character. In order to gain higher accuracy for the satellites,

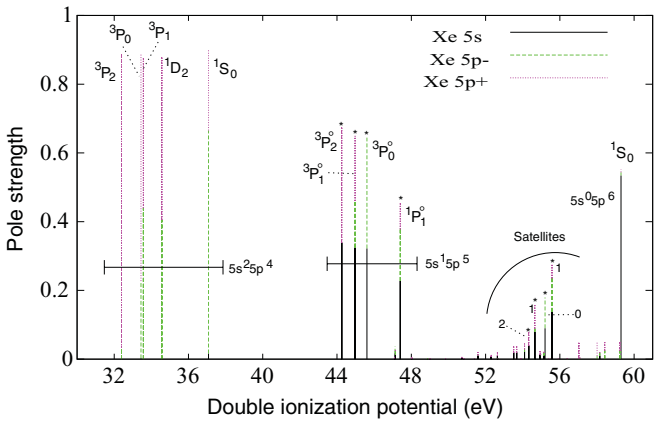

FIG. 1. (Color online) Computed double ionization spectrum of Xe. The contributions of different spinors to the pole strengths are distinguished by different colors. The numbers alongside the satellite states correspond to the J values. The states marked by asterisks are discussed in detail in the text.

TABLE II. Composition of the $^1P^o_1$ singlet states appearing at 47.41 and 55.58 eV in the calculated double ionization spectrum of Xe (see Fig. 1). The numbers are given in percent and correspond to the squared eigenvector coefficients multiplied by one hundred. The most relevant contributions are in bold face.

Config.	$\|\Psi(^1P^o_1)\rangle_\alpha$	$\|\Psi(^1P^o_1)\rangle_\beta$
$5s^15p^5$	**45.5**	**27.5**
$5s^05p^56s$	0.3	0.4
$5s^05p^55d$	0.2	0.6
$5s^05p^57s$	0.1	0.09
$5s^05p^56d$	0.1	0.1
$5s^15p^46p$	3.2	2.6
$5s^15p^44f$	0.2	0.5
$5s^15p^47p$	0.6	0.6
$5s^15p^45f$	0.0	0.04
$5s^25p^36s$	0.3	3.8
$5s^25p^35d$	**45.8**	**62.1**
$5s^25p^37s$	0.05	0.02
$5s^25p^36d$	2.6	0.5

a higher-order ADC method is needed, which is currently not available.

The last group of lines starts at 59.29(26.90) eV and is nearly completely composed of xenon $5s_{1/2}$ spinors, indicating states derived from the $5s^05p^6$ configuration. As for the dominating $5s^15p^5$ states, the intensity of the $5s^05p^6(^1S_0)$ state is reduced noticeably, indicating strong configuration interaction effects.

In the following, we will perform an eigenvector analysis of the most important states originating from the $5s^15p^5$ configuration and we intend to resolve a somehow misleading statement concerning the singlet-triplet splitting in this manifold. All the states for which eigenvectors were analyzed are marked by an asterisk in Fig. 1. From nonrelativistic theory, we would expect the $5s^15p^5(^3P^o_J)$ and $(^1P^o_1)$ terms, where the former undergoes a further spin-orbit splitting in a relativistic treatment. As seen from Fig. 1, all these states possess nearly equal atomic populations of the $5p$ and $5s$ spinors. The ratio between the $5p_{1/2}$ and $5p_{3/2}$ spinors varies, however, with the J value. From our calculations, we obtain the first singlet state of the $^1P^o_1$ character at 47.41(15.01) eV being 3.16 eV apart from the lowest $^3P^o_2$ triplet state.

Compared to the final states in the $5s^25p^4$ ground-state configuration, the $5s^15p^5$ final states have lost considerable intensity to a multitude of satellites. In the experiment, a large number of states originating from the $5s^25p^3nl$ shake-up configurations was observed [16], which energetically overlap with the $5s^15p^5$ configurations. Hereby, the odd-parity terms from the $5s^25p^35d$ and $5s^25p^36s$ configurations are the most suitable ones for a coupling to the $5s^15p^5$ terms. Although the $5s^25p^36p$ and $5s^25p^34f$ configurations also energetically overlap with the $5s^15p^5$ ones, they are of even parity that excludes any mixing between these configurations. The next odd-parity manifold ($5s^25p^36d$) is energetically far apart and can be neglected in the coupling. For a better understanding of the multiconfiguration effects, we therefore have to analyze the mixing between the $5s^15p^5$ main states and the $5s^25p^35d$-$5s^25p^36s$ shake-up configurations. The required information can be extracted from the $3h1p$ part of the ADC eigenvector, where each component represents the coefficient of a contributing $3h1p$ configuration to the final state under consideration. It should be mentioned that these $3h1p$ configurations do not represent pure Slater determinants but are to be understood as intermediate state representation (ISR) vectors. The leading contribution to such an ISR vector, however, consists of the corresponding $3h1p$ Slater determinant (see Ref. [49] for further details on ISR).

In the xenon case, we localize the most prominent satellite lines in the region between 54.3 and 55.6 eV (marked by asterisks in Fig. 1). An analysis of the corresponding $3h1p$ entries of the eigenvectors revealed the dominant contributions of the $5s^25p^35d^1$ and $5s^25p^36s^1$ configurations, which allows us to interpret these states as shake-up excitations accompanying ionization of the two outermost electrons. The high intensity acquired by these satellites arises due to their interactions with the main $5s^15p^5$ states, as indicated by the pronounced admixtures of the $5s^15p^5$ configurations. By inspection of the satellite $2h$ contributions, one also observes that the ratios between the $5s$ and $5p$ spinors there have a resemblance to the corresponding ratios in the main $5s^15p^5$ states. Thus, we arrive at the indicated correspondence of dominating states and associated satellites (their J quantum numbers are attached to the peaks). The main $5s^15p^5(^3P^o_{0,1,2})$ and $(^1P^o_1)$ states possess, in their turn, considerable contributions from the $5s^25p^35d^1$ and $5s^25p^36s^1$ configurations. For example, the eigenvector corresponding to the odd-parity triplet state $^3P^o_2(M_J=0)$ at 44.25(11.86) eV has the following appearance:

$$\Psi\left(^3P^o_2\right) = -0.582\left|5p_{\frac{3}{2},-\frac{1}{2}}5s_{\frac{1}{2},\frac{1}{2}}\right| + 0.180\left|5p_{\frac{3}{2},-\frac{3}{2}} \times 5p_{\frac{3}{2},-\frac{1}{2}}5p_{\frac{3}{2},\frac{1}{2}}5d_{\frac{3}{2},\frac{3}{2}}\right| + \ldots,$$

where only the leading $2h$ and the leading $3h1p$ contributions are shown. We also note that in this configurational expansion, the Kramers-reversed linear combinations occur with the same coefficients as the original ones, where the Kramers partner of a spinor is obtained by negating its m_j component (e.g., $p_{\frac{3}{2},\frac{1}{2}} \rightarrow p_{\frac{3}{2},-\frac{1}{2}}$).

The loss of intensity of the $^1P^o_1$ singlet state at 47.41(15.01) eV is even more pronounced than of the triplet states, which posed a difficulty with its proper assignment as discussed in the Introduction. It exhibits the strongest interaction with another $^1P^o_1$ state at 55.58(23.18) eV. The corresponding experimental lines lie at 47.86(14.76) and 53.38(20.27) eV, respectively [16,26]. By performing configuration interaction calculations, Persson *et al.* [16] found that these states possess nearly the same percentages of the $5s^15p^5$ configurations, namely 28% and 27%, respectively, while the contributions of the $5s^25p^3(^2D)5d$ configurations differ remarkably (44% vs. 33%). The first $^1P^o_1$ state was therefore interpreted as a satellite and the second as the main state. As long as the LS coupling scheme can be maintained, a unique classification of the lowest-energy singlet state is important for the determination of the singlet-triplet splitting within the $5s^15p^5$ configuration. By adopting the Persson's assignment, one would therefore arrive at the $^1P^o_1 - {}^3P^o_2$ splitting of 8.09 eV, which seems to be quite exaggerated compared to the trends in the lighter homologues (see Table III).

In order to obtain deeper insight into the nature of the aforementioned states, we performed a detailed eigenvector analysis comprising the $3h1p$ parts of the ADC eigenvectors. Let us term the eigenvectors corresponding to the states at 47.41 and 55.58 eV in Fig. 1 as $|\Psi(^1P^o_1)\rangle_\alpha$ and $|\Psi(^1P^o_1)\rangle_\beta$, respectively. The leading terms of the $|\Psi(^1P^o_1)\rangle_\alpha$ eigenvector are

$$\begin{aligned}\left|\Psi\left(^1P^o_1\right)\right\rangle_\alpha = &-0.388\left(\left|5p_{\frac{1}{2},\frac{1}{2}}5s_{\frac{1}{2},-\frac{1}{2}}\right| + \left|5p_{\frac{1}{2},-\frac{1}{2}}5s_{\frac{1}{2},\frac{1}{2}}\right|\right)\\ &+0.277\left(\left|5p_{\frac{3}{2},\frac{1}{2}}5s_{\frac{1}{2},-\frac{1}{2}}\right| + \left|5p_{\frac{3}{2},-\frac{1}{2}}5s_{\frac{1}{2},\frac{1}{2}}\right|\right)\\ &+0.274\left(\left|5p_{\frac{3}{2},\frac{3}{2}}5p_{\frac{3}{2},\frac{1}{2}}5p_{\frac{1}{2},\frac{1}{2}}5d_{\frac{5}{2},-\frac{5}{2}}\right|\right.\\ &\left.+\left|5p_{\frac{3}{2},-\frac{3}{2}}5p_{\frac{3}{2},-\frac{1}{2}}5p_{\frac{1}{2},-\frac{1}{2}}5d_{\frac{5}{2},\frac{5}{2}}\right|\right) + \ldots\end{aligned}$$

TABLE III. Minimum and maximum singlet-triplet splitting ($\Delta^{\mathrm{ST}}_{\mathrm{min}}$, $\Delta^{\mathrm{ST}}_{\mathrm{max}}$) in the ns^1np^5 manifold for the noble gases ($n = 2\cdots5$).

Atom	$\Delta^{\mathrm{ST}}_{\mathrm{min}}$	$\Delta^{\mathrm{ST}}_{\mathrm{max}}$
Ne	10.67	10.79
Ar	4.23	4.43
Kr	3.12	3.84
Xe	1.80	3.16

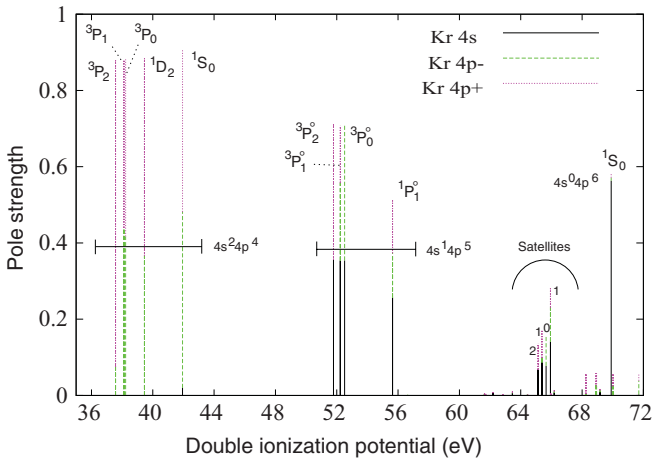

FIG. 2. (Color online) Computed double ionization spectrum of Kr. The contributions of different spinors to the pole strengths are distinguished by different colors. The numbers alongside the satellite states correspond to the J values.

Note that the sum of all squared coefficients in an ADC eigenvector yields unity due to a normalization condition. From the eigenvector analysis above, one can see that contributions from specific (j,m_j) spinors can be individually addressed, which makes this method very useful. For practical purposes, however, one may be more interested in contributions grouped in terms of l quantum numbers without a distinction between $l \pm \frac{1}{2}$. In Table II, all important contributions for $|\Psi(^1P_1^o)\rangle_\alpha$ and $|\Psi(^1P_1^o)\rangle_\beta$ are listed according to the l-grouping together with their weights in percent allowing for their precise characterization. The contributions due to the $5s^15p^5$ and $5s^25p^35d$ configurations representing particular interest are shown in bold.

When examining the state $|\Psi(^1P_1^o)\rangle_\alpha$ separately, one would not be able to make a definite assignment of its character as this state contains nearly equal contributions of the most important $5s^15p^5$ and $5s^25p^35d$ configurations. However, since the contribution of the $5s^15p^5$ configuration in this state is by far the biggest one among all the states (the second largest contribution (27.5%) of the $5s^15p^5$ configuration is found in the state $|\Psi(^1P_1^o)\rangle_\beta$ as seen from Table II and Fig. 1), we can conclude with confidence that this state represents the main $5s^15p^5(^1P_1^o)$ singlet state in agreement with the Moore's classification [24]. Correspondingly, the state $|\Psi(^1P_1^o)\rangle_\beta$ obeying the prevailing configuration $5s^25p^35d$ is assigned as a satellite. The singlet-triplet splitting $^1P_1^o - ^3P_2^o$ thus amounts to 3.16 eV.

B. Krypton, argon, and neon

In this subsection, we compare the xenon results to the double ionization spectra of the lighter homologues krypton, argon, and neon. The krypton and argon spectra (see Figs. 2 and 3) show structures that are very similar to those in the spectrum of xenon. When going from Xe to Ar, the spin-orbit splittings of both the triplet states $ns^2np^4(^3P_J)$ and $ns^1np^5(^3P_J^o)$ ($n = 5,4,3$ for xenon, krypton, and argon, respectively) into the $J = 0,1,2$ multiplets decrease, which is correctly reproduced by our calculations. Note the reverse ordering of the $ns^2np^4(^3P_0)$ and $(^3P_1)$ states in the spectra of the lighter ions. Due to strong configuration interaction effects the $ns^1np^5(^3P_J^o)$ and $(^1P_1^o)$ characters are distributed over a number of satellite states. The most intense ones are found in the energy interval between 65 and 66 eV in the krypton spectrum and between 73 and 75 eV the spectrum of argon. By analyzing the $2h$ parts of these satellites, one can

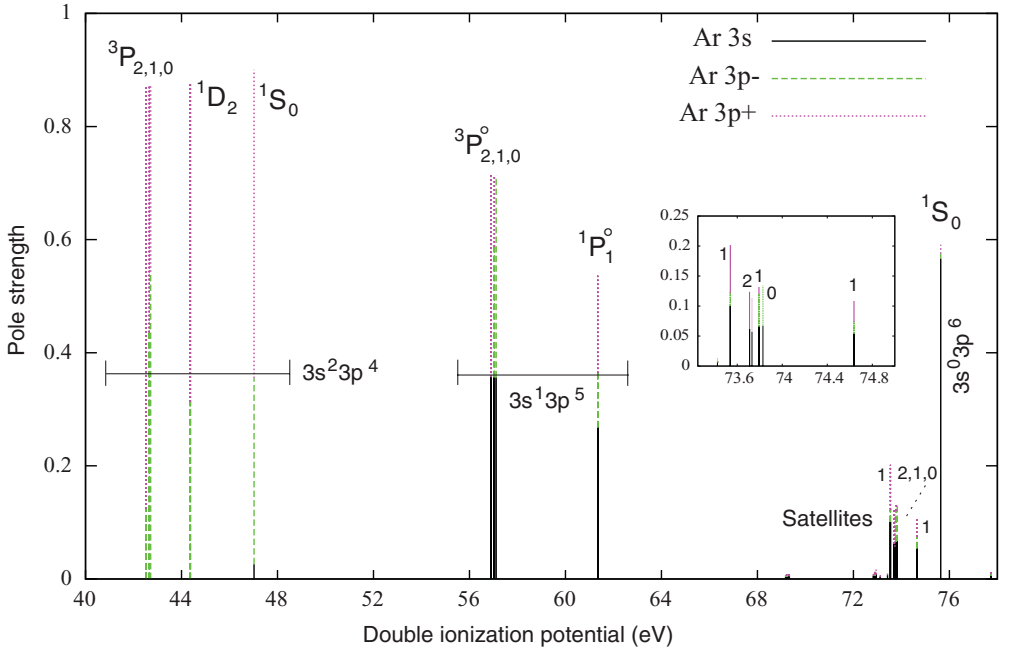

FIG. 3. (Color online) Computed double ionization spectrum of Ar. The contributions of different spinors to the pole strengths are distinguished by different colors. The numbers alongside the satellite states correspond to the J values. The energy region containing the most intense satellites is expanded in the inset. Note the splitting of the $^1P_1^o$ state due to a configuration interaction.

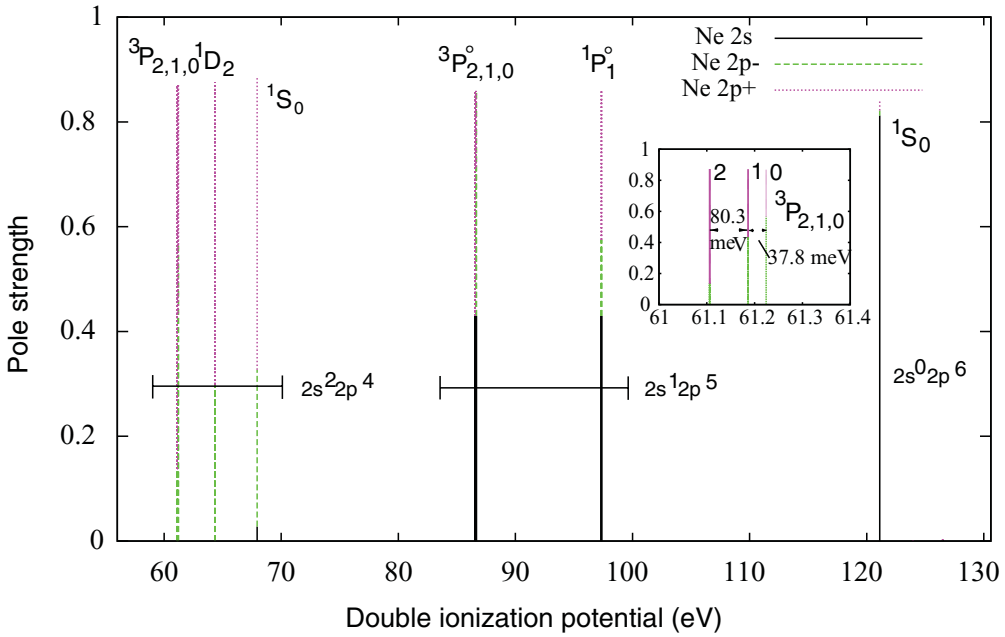

FIG. 4. (Color online) Computed double ionization spectrum of Ne. The contributions of different spinors to the pole strengths are distinguished by different colors. The inset shows a close-up of the $2s^2 2p^4(^3P_{2,1,0})$ triplet manifold split by spin-orbit coupling.

identify the corresponding $^3P^o_{2,1,0}$ and $^1P^o_1$ parent states. The $3h1p$ parts provide information on the configurations involved in the interactions. These configurations are similar to those addressed in the previous subsection when Xe was discussed, only the principal quantum numbers are smaller by one and two in the case of krypton and argon, respectively. Although the pole strengths of the $ns^1np^5(^1P^o_1)$ states in the Kr and Ar spectra are noticeably reduced relative to all other main states, they appear to be higher than the pole strength of the respective state in the spectrum of Xe III. Consequently, the interpretation of the Kr and Ar spectra meets less difficulties. Finally, the computed energy differences between the $^1P^o_1$ and $^3P^o_2$ states of Kr III and Ar III constitute 3.84 and 4.43 eV, respectively. This singlet-triplet splitting increases dramatically in the Ne case.

The double ionization spectrum of Ne looks differently (see Fig. 4). The tiny spin-orbit coupling now allows the ^3P_J and $^3P^o_J$ final states to be classified as nearly pure triplets (see the smallness of the effect in the inset of Fig. 4). By using the threshold photoelectrons coincidence (TPEsCO) method, Avaldi *et al.* [9] could resolve for the first time the $2s^2 2p^4(^3P_{2,1,0})$ multiplet of Ne^{2+} with spacings of 80 and 35 meV. The corresponding calculated splittings amount to 80.3 and 37.8 meV and thus are in very good agreement to the experimental values.

Very high pole strengths and the absence of energetically close-lying intense shake-up states indicate that the multiconfiguration character of the main states of Ne^{2+} disappears completely. The $2s^1 2p^5(^1P^o_1)$ state is no longer repelled to lower energies due to interactions with satellites and the singlet-triplet splitting $^1P^o_1$-$^3P^o_2$ is rather high. Being the strongest in the noble gas series, it constitutes 10.7 eV. In Table III we list the computed minimum and maximum energetic gaps between the singlet and triplet terms (the difference between the maximum and minimum originates due to SO-coupling). By adopting the above interpretation for the main singlet $^1P^o_1$ state of Xe, we observe that the singlet-triplet splitting decreases in the sequence from Ne to Xe. In the case of radon (see below), no reasonable singlet-triplet interpretation can be maintained anymore.

As one can see from Fig. 4, all the main states in the neon spectrum exhibit very high pole strengths. After a convolution, e.g., with a Lorentzian profile, we obtain a double ionization spectrum reflecting statistical weights of each contributed state only. However, this spectrum differs dramatically from the experimental spectrum (see, for example, Refs. [9,13]), which shows the pronounced intensity decrease when going from outer-valence to inner-valence spectral regions. The intensity of the $2s^0 2p^6(^1S_0)$ state is particularly weak. This intensity decrease is not due to configuration interaction effects (these were not revealed in the calculations) but rather due to a double photoionization cross-section effect. In the present work, the above cross sections were not taken into account. We also did not consider indirect double ionization mechanisms, for instance, through autoionization of highly excited singly charged ions, which may strongly perturb the intensities.

C. Radon

At the end of the discussion we present the double ionization spectrum for radon (see Fig. 5). Only in the ground-state manifold of Rn^{2+} a dominant main-state character is visible. The J ordering of the (^3P_J) states is 2,0,1. Hereby, one easily recognizes that the spin-orbit splitting of this state is now of comparable size as the electrostatic repulsion responsible for the splitting into ^3P, ^1D, and ^1S terms. Therefore, a LS-based picture is erroneous for a proper interpretation of the spectrum. In Table IV we list the calculated double ionization potentials of the $6s^2 6p^4$ states relative to the ground state of the

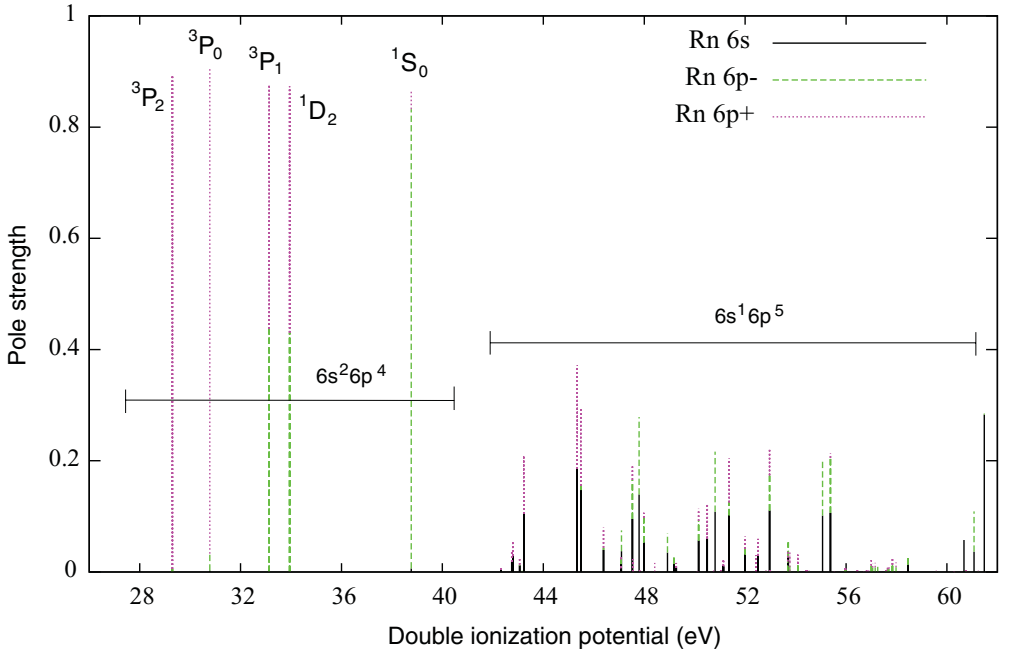

FIG. 5. (Color online) Computed double ionization spectrum of Rn. The contributions of different spinors to the pole strengths are distinguished by different colors. The *LS* assignments become inappropriate and are only given as an orientation.

radon dication, which agree nicely with the results of another theoretical calculation [42].

The pronounced multiconfigurational character in the $6s^16p^5$ manifold now does no longer reveal any systematic structure, and the intensities of the peaks are distributed over the whole range. We also performed a Rn^{2+} spectrum calculation under neglect of spin-orbit coupling that automatically gave a considerably reduced number of final states (not shown). Interestingly, the breakdown of the single configuration approach in the $6s^16p^5$ manifold pertained even in this case and no dominating states could be detected. Even in the absence of the spin-orbit coupling, many energetically close-lying shake-up states emerging from the Rn^{2+} ground-state configuration lead to a strong multiconfiguration character in the excited $6s^16p^5$ configuration of the dication.

As a final result we calculated averaged energetic shifts of the singly and doubly ionized main states where corrections to the Coulomb repulsion term were taken into account (Table V). In the Dirac program package [56] where the relativistic propagator is implemented, these corrections comprise the magnetic (Gaunt) term, whereas the Breit corrections are not yet available. The molecular spinors were hereby obtained by inclusion of the Gaunt-type integrals in addition to the Coulomb integrals. One can see an increasing contribution of the Gaunt term in heavier systems which stays well below 0.1 eV even for the radon atom. Relevant structural changes in the spectra or in state compositions were, however, not observed within the methodological accuracy.

TABLE IV. Calculated relative energies (in eV) of the main $6s^26p^4$ states of Rn III.

Term	J	This work	Ref. [42]
^3P	2	0.00	0.00
	0	1.48	1.39
	1	3.83	3.88
^1D	2	4.64	4.65
^1S	0	9.46	9.27

TABLE V. Average SIP and DIP energetic shifts in meV for the noble gas atoms upon inclusion of the Gaunt term.

Atom	SIP	DIP
Ne	4.0	3.6
Ar	4.1	4.5
Kr	6.8	8.8
Xe	9.0	13.3
Rn	18.7	26.2

V. SUMMARY

In this work, we have applied the relativistic two-particle propagator in the implementation of the algebraic diagrammatic construction to the calculation and interpretation of the noble gas double ionization spectra. A detailed final-state analysis in terms of the $2h$ and $3h1p$ eigenvector components allowed for a unique configurational characterization of the individual lines. Considerable multiconfiguration effects in the excited $5s^15p^5$ Xe^{2+} manifold caused some ambiguity in the assignment of the $^1P_1^o$ singlet state and could be resolved by our final-state analysis. In the series from neon to radon, multiconfiguration effects increase substantially in the ns^1np^5 regime, whereas the ground-state ns^2np^4 configurations retain their main-state character in all systems. In addition, the $^1P_1^o$ – $^3P_J^o$ singlet-triplet splitting continuously decreases from Ne to Xe, where it should be noted that the notion of a triplet becomes more and more inappropriate when going from light to heavy

systems. In radon, spin-orbit and multiconfiguration effects are so large that a spectrum calculation will be erroneous in a nonrelativistic and even scalar-relativistic framework emphasizing the requirement of four-component propagators.

ACKNOWLEDGMENTS

M.P. and N.V.K. gratefully acknowledge financial support by the Deutsche Forschungsgemeinschaft.

[1] F. M. Harris, Int. J. Mass Spectrom. Ion Processes **120**, 1 (1992).
[2] K. Vékey, Mass Spectr. Rev. **14**, 195 (1995).
[3] P. Lablanquie, S.-M. Huttula, M. Huttula, L. Andric, J. Palaudoux, J. H. D. Eland, Y. Hikosaka, E. Shigemasa, K. Ito, and F. Penent, PhysChemChemPhys. **13**, 18355 (2011).
[4] Y. Hikosaka, P. Lablanquie, F. Penent, T. Kaneyasu, E. Shigemasa, J. H. D. Eland, T. Aoto, and K. Ito, Phys. Rev. Lett. **98**, 183002 (2007).
[5] A. E. Kramida and G. Nave, Eur. Phys. J. D **37**, 1 (2006).
[6] J. H. D. Eland, O. Vieuxmaire, T. Kinugawa, P. Lablanquie, R. I. Hall, and F. Penent, Phys. Rev. Lett. **90**, 053003 (2003).
[7] T. X. Carroll, J. D. Bozek, E. Kukk, V. Myrseth, L. J. Sæthre, T. D. Thomas, and K. Wiesner, J. Electron Spectrosc. Relat. Phenom. **125**, 127 (2002).
[8] P. Bolognesi, S. J. Cavanagh, L. Avaldi, R. Camilloni, M. Zitnik, M. Stuhec, and G. C. King, J. Phys. B **33**, 4723 (2000).
[9] L. Avaldi, G. Dawber, N. Gulley, H. Rojas, G. C. King, R. Hall, M. Stuhec, and M. Zitnik, J. Phys. B **30**, 5197 (1997).
[10] H. Pulkkinen, S. Aksela, O. P. Sairanen, A. Hiltunen, and H. Aksela, J. Phys. B **29**, 3033 (1996).
[11] L. Avaldi, G. Dawber, G. C. King, G. Stefani, and M. Zitnik, Phys. Rev. A **52**, R3409 (1995).
[12] J. Jauhiainen, H. Aksela, S. Aksela, A. Kivimäki, O. P. Sairanen, E. Nõmmiste, and J. Végh, J. Phys. B **28**, 3831 (1995).
[13] R. I. Hall, G. Dawber, A. G. McConkey, M. A. MacDonald, and G. C. King, Z. Phys. D **23**, 377 (1992).
[14] W. Persson, C.-G. Wahlström, L. Jönsson, and H. O. Di Rocco, Phys. Rev. A **43**, 4791 (1991).
[15] S. D. Price and J. H. D. Eland, J. Phys. B **22**, L153 (1989).
[16] W. Persson, C.-G. Wahlström, G. Bertuccelli, H. O. Di Rocco, J. G. Reyna Almandos, and M. Gallardo, Phys. Scr. **38**, 347 (1988).
[17] H. Aksela, S. Aksela, and H. Pulkkinen, Phys. Rev. A **30**, 865 (1984).
[18] S. Southworth, U. Becker, C. M. Truesdale, P. H. Kobrin, D. W. Lindle, S. Owaki, and D. A. Shirley, Phys. Rev. A **28**, 261 (1983).
[19] K. G. Dyall and F. P. Larkins, J. Phys. B **15**, 2793 (1982).
[20] H. Hertz, Z. Phys. A **274**, 289 (1975).
[21] E. J. McGuire, Phys. Rev. A **11**, 17 (1975).
[22] L. O. Werme, T. Bergmark, and K. Siegbahn, Phys. Scr. **8**, 149 (1973).
[23] L. O. Werme, T. Bergmark, and K. Siegbahn, Phys. Scr. **6**, 141 (1972).
[24] C. E. Moore, Atomic Energy Levels, Vol. III (US Government Printing Office, Washington DC, 1971).
[25] E. B. Saloman, J. Phys. Chem. Ref. Data **33**, 765 (2004).
[26] Y. Ralchenko, A. E. Kramida, J. Reader, and NIST ASD Team, NIST Atomic Spectra Database (ver. 4.1.0) (National Institute of Standards and Technology, Gaithersburg, 2011).
[27] J. Schirmer and A. Barth, Z. Phys. A **317**, 267 (1984).
[28] A. Tarantelli and L. S. Cederbaum, Phys. Rev. A **39**, 1656 (1989).
[29] F. Tarantelli, L. S. Cederbaum, and A. Sgamellotti, J. Electron Spectrosc. Relat. Phenom. **76**, 47 (1995).
[30] F. Tarantelli, Chem. Phys. **329**, 11 (2006).
[31] M. Pernpointner, S. Urbaczek, and N. V. Kryzhevoi, J. Chem. Phys. **129**, 024304 (2008).
[32] E. Faßhauer, N. V. Kryzhevoi, and M. Pernpointner, J. Chem. Phys. **130**, 014303 (2010).
[33] M. Pernpointner, J. Phys. B **43**, 205102 (2010).
[34] I. P. Grant, B. J. McKenzie, P. H. Norrington, D. F. Mayers, and N. C. Pyper, Comput. Phys. Commun. **21**, 207 (1980).
[35] P. Jönsson, X. He, C. Froese-Fischer, and I. P. Grant, Comput. Phys. Commun. **177**, 597 (2007).
[36] S. Fritzsche, C. Froese-Fischer, and G. Gaigalas, Comput. Phys. Commun. **148**, 103 (2002).
[37] X.-B. Ding, F. Koike, I. Murakami, D. Kato, H. A. Sakaue, C.-Z. Dong, N. Nakamura, A. Komatsu, and J. Sakoda, J. Phys. B **44**, 145004 (2011).
[38] C. Froese-Fischer, J. Phys. B **43**, 074020 (2010).
[39] X.-L. Wang, S.-H. Chen, X.-Y. Han, and J.-M. Li, Chin. Phys. Lett. **25**, 903 (2008).
[40] T. Brage, C. Proffitt, and D. S. Leckrone, Astrophys. J. **513**, 524 (1999).
[41] M. J. Vilkas and Y. Ishikawa, J. Phys. B **37**, 1803 (2004).
[42] E. Biémont and P. Quinet, Phys. Scr. **54**, 36 (1996).
[43] G. E. Brown and D. G. Ravenhall, Proc. R. Soc. London A **208**, 552 (1951).
[44] J. Sucher, Phys. Rev. A **22**, 348 (1980).
[45] G. Pestka, M. Bylicki, and J. Karwowski, J. Phys. B **39**, 2979 (2006).
[46] M. Bylicki, G. Pestka, and J. Karwowski, Phys. Rev. A **77**, 044501 (2008).
[47] I. P. Grant and H. M. Quiney, Adv. At. Mol. Phys. **23**, 37 (1988).
[48] H. Lehmann, Nuovo Cimento **11**, 342 (1954).
[49] J. Schirmer, Phys. Rev. A **43**, 4647 (1991).
[50] J. Schirmer, L. S. Cederbaum, and O. Walter, Phys. Rev. A **28**, 1237 (1983).
[51] L. S. Cederbaum, W. Domcke, J. Schirmer, and W. von Niessen, Adv. Chem. Phys. **65**, 115 (1986).
[52] J. Schirmer, L. S. Cederbaum, W. Domcke, and W. von Niessen, Chem. Phys. Lett. **57**, 582 (1978).
[53] K. G. Dyall, Theor. Chem. Acc. **108**, 335 (2002).
[54] K. G. Dyall, Theor. Chem. Acc. **109**, 284 (2003).
[55] K. G. Dyall, Theor. Chem. Acc. **115**, 441 (2006).
[56] DIRAC, a relativistic ab initio electronic structure program, Release DIRAC10 (2010), written by T. Saue, L. Visscher and H. J. Aa. Jensen, with contributions from R. Bast, K. G. Dyall, U. Ekström, E. Eliav, T. Enevoldsen, T. Fleig, A. S. P. Gomes, J. Henriksson, M. Iliaš, Ch. R. Jacob, S. Knecht, H. S. Nataraj, P. Norman, J. Olsen, M. Pernpointner, K. Ruud, B. Schimmelpfennig, J. Sikkema, A. Thorvaldsen, J. Thyssen, S. Villaume, and S. Yamamoto [see http://dirac.chem.vu.nl].